Numerical life estimation after fatigue failure of a complex component

J. L. OTEGUI[1], H. LÓPEZ MONTENEGRO[1] and A. A. MÁRQUEZ[2]

[1]*INTEMA, CONICET, University of Mar del Plata, Juan B. Justo 4302, 7600 Mar del Plata, Argentina;* [2]*GIE S.A., Camusso 30, 7600 Mar del Plata, Argentina*

Received in final form 23 February 2005

ABSTRACT Failure of a large ethylene-reciprocating compressor was found to be due to fatigue growth of cracks in the crosshead of one of the cylinders, initiated at material defects near stress raisers. Total fatigue crack growth time was required in order to identify the cause of the failure. The applied stress field near the initiation sites and along fatigue path was estimated using FEM. The stresses were found to vary steeply and become partly compressive along a large part of the fatigue crack path. A weight function based on numerical method was developed, which was able to predict exactly the shape of the crack front during propagation. Fatigue crack initiation was traced to a disassembly 6 months before final failure. This failure was found to be jointly the result of non-conformities in manufacture and maintenance.

Keywords defect assessment; fatigue failure; large industrial component; numerical modelling.

INTRODUCTION

This work describes the methodology developed to determine the origin and reasons of a major failure in an ethylene compressor in a petrochemical plant. The compressor had been installed less than 2 years before, and its total number of rotation cycles up to failure was estimated to be 350 million. This failure, as with many other non-redundant components in plants subject to continuous operation, caused serious operative and economic damage. The determination of the cracking mechanisms was fundamental for the prevention of future failures. The reciprocating compressor has two cylinders, and failed after the crosshead and crosshead liner of cylinder B broke. Subsequent turns of moving parts (especially the connecting rod of cylinder B) provoked massive damage to the crankcase and other parts. Figure 1 shows a diagram of parts related to the crosshead of cylinder B.

Since its installation this part of the machine had been disassembled several times to correct some abnormalities including: rust in the piston cylinder produced before service, and abnormal wear in piston rings, produced twice during service. Two weeks before failure, maintenance personnel had worked on the machine to replace the piston rings. The operator, insurance company and manufacturer of this equipment arranged a joint task force in order to define causes, mitigation measures and contractual responsibilities. Central to this study was to precisely date the crack initiation. As it will be seen, this involved defining the applied cyclic stress intensity factor ranges in a region with steep stress gradients, experimentally determining material fatigue properties and sizing initiation defects.

Correspondence: J. L. Otegui. E-mail: jotegui@fi.mdp.edu.ar; A.A. Márquez. E-mail: marquez@giemdp.edu.ar

CHARACTERIZATION OF MATERIAL PROPERTIES AND CRACK INITIATION SITES

A failure analysis was carried out, by analysing the characteristics of several cracks and other defects present in the affected pieces, defining material properties and performing mechanical modelling.[1] The crosshead material is a C–Mn GS45 cast steel, with 0.5% Si and 0.1% Cr, and a nominal ultimate tensile strength of 450 MPa. Impact Charpy V-notch test results of crosshead material show that at room temperature this material is within the ductile to brittle transition range. Lower bound fracture toughness for this material was estimated from the impact results. The fracture toughness drops from more than 100 MPa $m^{1/2}$ at 80 °C to less than 30 MPa $m^{1/2}$ at room temperature. The instant when the crosshead takes the maximum load at minimum temperature is at its start up cycle.

The failed crosshead and related parts were subjected to visual and fractographic analysis, and several defects and

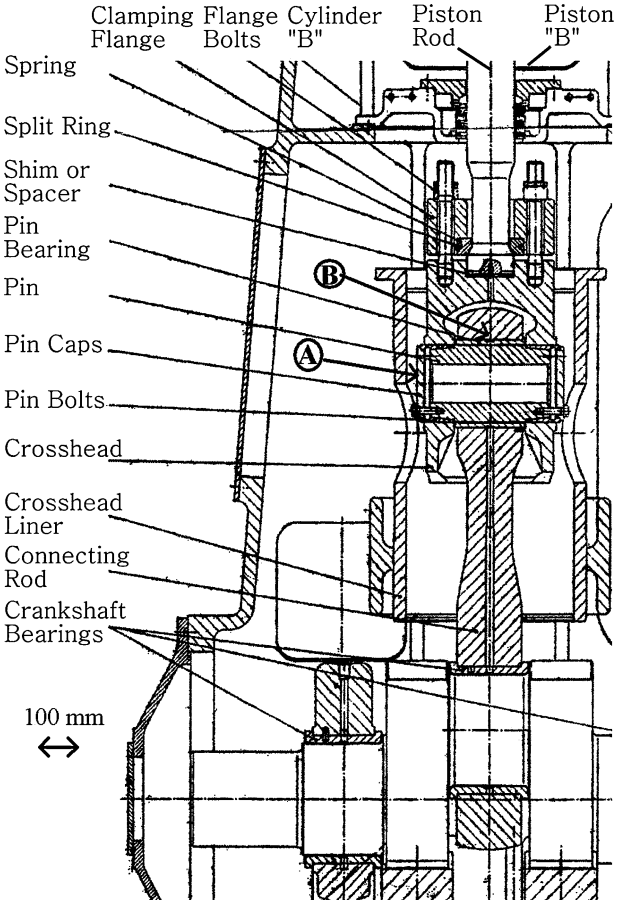

Fig. 1 Diagram of parts related to the failed crosshead in a large reciprocating compressor.

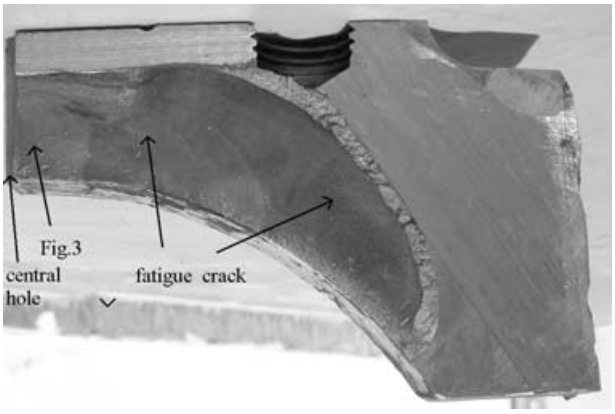

Fig. 2 Remaining crack in the upper part of crosshead.

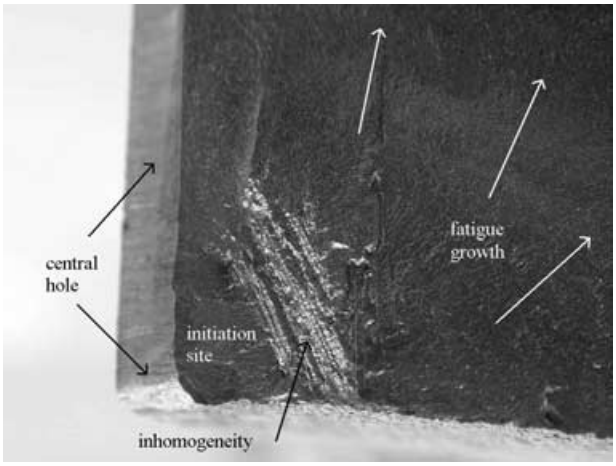

Fig. 3 (×3) Material defect at initiation site of remaining crack.

abnormalities were identified. The failure of the crosshead was due to a perimetral crack that developed between the pinholes in the crosshead. This is called the main crack, and is indicated as A in the sketch of Fig. 1. The complete fracture of the crosshead occurred when this horizontal crack became unstable under applied operating loads, the crosshead fractured in the section between the pinholes, and produced the final failure of the equipment. This caused major damage in most of the compressor, including bursting of the crosshead liner, several fractures in the crankcase, permanent deformations in the cylinder rod and other components. Another crack was found in a vertical plane in the upper part of the crosshead, which is called the remaining crack because it did not fracture completely. The position of this remaining crack is indicated as B in the sketch of Fig. 1.

The shape and location of the remaining crack was identified by ultrasonic inspection. Then the piece containing the crack was cut and frozen in dry ice to open the crack surfaces. It was found that not one elliptical crack but two symmetrical corner cracks had initiated from opposite sides of a central 5-mm hole in the upper part of the crosshead. One of these remaining cracks is seen in Fig. 2. Fatigue beach marks are visible, initiated near the bottom end of the central bore. Neither crack reached the nearby bore for the bolts that fix the rod clamping flange to the crosshead. There are indications of material inhomogeneities at the initiation sites of both remaining cracks, see for example Fig. 3 (X3). Unfortunately, the initiation site of the main crack between the pinholes was completely deformed due to impacts against the connecting rod after fracture of the crosshead, so no identification of initial defects was possible.

Slices were cut from these regions, and at the initiation site of the main crack, and inspected in a scanning electron microscope. Several metallographic specimens were prepared, at planes parallel and normal to the crack surface. Fatigue striations are seen in most of the fracture surfaces of all cracks (remaining and main). Figure 4 (×1000) shows indications of fatigue striations in one of the remaining cracks, which confirm the crack growth mechanism far

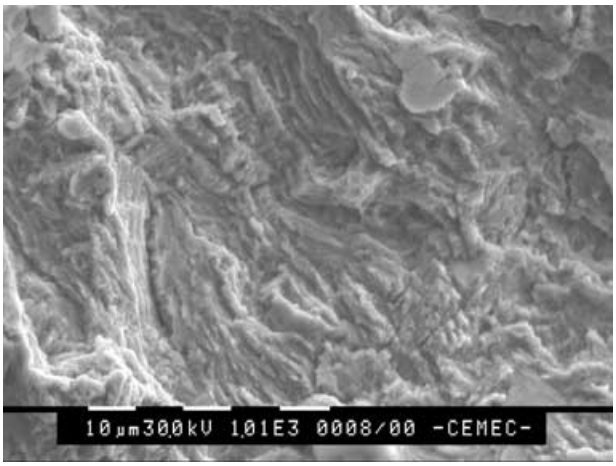

Fig. 4 (×1000) Fatigue striations in the fracture surface of the remaining crack.

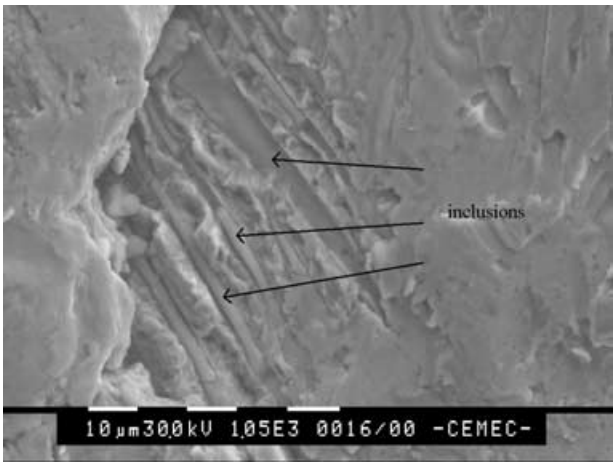

Fig. 5 (×1000) Intergranular propagation of discontinuities at the initiation site of the remaining crack.

from the initiation sites. Striation spacing is between 1 and 2 μm. Most of the indications in the fracture surfaces of the remaining cracks (close to the central hole), however, point to intergranular cracking.

The material discontinuities seen in Fig. 3 are the largest defects in the region, indicating interdendritic voids formed during solidification of the cast steel. What is seen in Fig. 5 (×1000) is some intergranular propagation in the material between the voids and the central hole (Fig. 2). Note the small diameter, elongated cylindrical particles included within the branches in the matrix. These are non-metallic inclusions.

Indications of fatigue striations are also apparent in the fatigue growth side of the main crack, between the pinholes in the lower part of the crosshead. Again, fatigue is confirmed as the propagation mechanism. Spacing between striations is around 2 μm about 50 mm from initiation site, and 15 μm about 20 mm from initiation site. It can be speculated that the fatigue crack growth rate was faster near initiation due to the stress concentration at the pinhole. Initiation sites at the pinhole were severely deformed by the connecting rod after failure, and therefore no fractographic analysis is possible in this region.

The fracture mechanics estimation of the required propagation time for a fatigue crack to grow from an initial crack size to a final crack size was done by using the cyclic stress intensity factor ΔK, and applying the Paris equation for fatigue propagation[2]: $\mathrm{d}a/\mathrm{d}N = C\ \Delta K^m$. Values of C and m defined in the literature for these steels depend on several factors such as material strength and ductility, grain size, distribution of defects and inclusions, mean stress, environment, etc. In order to more accurately model the time required for the fatigue cracks to grow, an experimental assessment of fatigue crack growth parameters in the material of the crosshead was carried out, according to ASTM E647,[3] with a minimum-to-maximum load ratio $R = 0.2$.

When the crack growth rate $\mathrm{d}a/\mathrm{d}N$ is measured in m cycle^{-1}, experimental results are $C = 2.257\ 10^{-12}$, $m = 3.287$, $\Delta K_{\mathrm{th}} = 4.278$ MPa m$^{1/2}$. For large applied ΔK values these values give larger propagation rates than those defined in the literature for ferritic pearlitic steels.[2] These correspond to the low-cycle fatigue regime. In the very large cycle fatigue regime, that is, for ΔK values close to threshold, experimental constants predict fatigue growth rates almost half those from the literature.

NUMERICAL PROCEDURE

The 'O-Integral' weight function

The algorithm known as 'O-Integral', was developed by Oore and Burns[4] to calculate the applied opening mode stress intensity factor (SIF) at the front of irregular planar cracks embedded in an infinite solid. As it can be seen from Fig. 6a, the SIF $K_{QQ'}$ at any point Q' in the crack front, produced by a pair of symmetric opening forces P_Q acting at point Q on the crack surfaces, is given by

$$K_{QQ'} = P_Q \cdot W_{QQ'}, \tag{1}$$

where $W_{QQ'}$ is the SIF at Q', per unit force at Q. This is termed the weight function (WF), and only depends on the problem geometry.[5] Given that most of the available weight function solutions are restricted to two-dimensional cracks and regular crack geometries in three dimensions,[6] the scope of problems which can be solved using this technique is limited.

In an effort to extend the applicability of weight function methodology, Oore and Burns[4] examined the structure of the weight functions for three-dimensional cracks for which there are known solutions, and surmised that in

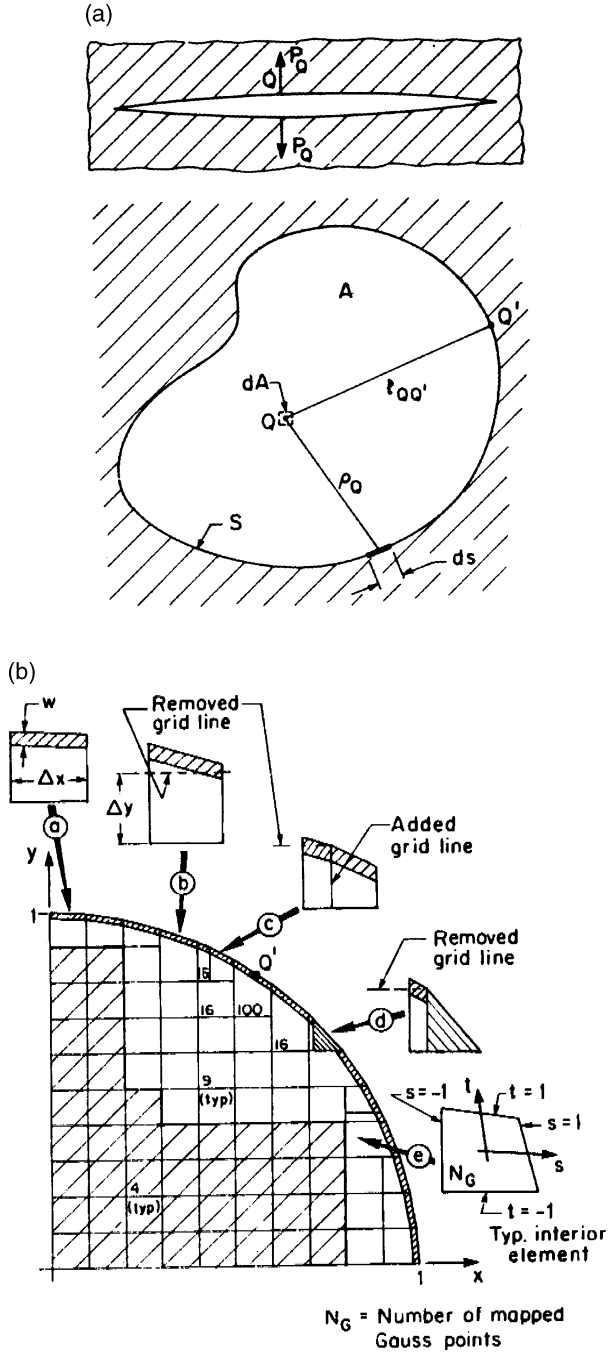

Fig. 6 (a) Irregular planar crack embedded in an infinite solid and variables definition. (b) Quarter ellipse discretization dimensionless (x, y) *coordinates*.

general these weight functions could be rewritten as the following algorithm, termed the O-Integral:

$$W_{QQ'} = \frac{\sqrt{2}}{\pi \cdot l_{QQ'}^2} \cdot \frac{1}{\left[\int_S \frac{ds}{\rho_Q^2}\right]^{1/2}}, \tag{2}$$

where $l_{QQ'}$ is the distance from the load point Q to the point Q' on the crack front, and ρ_Q is the distance from Q to the centre of the elemental length ds of the crack front s (see Fig. 6a). For any opening stress σ_Q acting on the crack surfaces, the SIF $K_{Q'}$ at point Q' is an integral calculated on the crack surface area A:

$$K_{Q'} = \int_A \sigma_Q \cdot W_{QQ'} \cdot \mathrm{d}A. \tag{3}$$

The O-Integral WF exactly matches closed form solutions for circular and semiinfinite straight front cracks in infinite solids.[4] The O-Integral also gives satisfactory results for embedded rectangular and some irregular cracks with a front line that changes from concave to convex curvature.[7] An efficient computational O-Integral approach for irregular crack front geometries was later developed with a hybrid numerical–analytical integration technique.[8,9] The technique considers differentiated interior and boundary elements (see Fig. 6b for the discretization of a quarter circumference). Calibration studies were performed for embedded and surface cracks under membrane and bending stresses. The maximum error is near to 18%, and corresponds to the ends of the major axis in surface cracks. This error is due to the O-Integral itself, not to the integration procedure.[7]

The Calsyf program

A correction function was needed in order to obtain satisfactory SIF solutions. The program 'Calsyf'[10] overcomes this problem and allows the calculation of the SIF for embedded and surface cracks in an infinite solid and in plates. The correction function was developed by comparison of exact solutions for ellipses of different aspect ratios under uniform stress,[11] and using a numerical technique similar to that of Desjardins, but with a more efficient discretization subroutine. Numerical solutions for rectangular cracks were also used.[12] The program Calsyf incorporates the correction function to the O-Integral result for cracks embedded in an infinite volume as well as another correction factor that takes account of the presence of a free surface when treating surface cracks and finite boundaries. These last corrections were obtained from the known solutions of Newman–Raju.[13,14]

Crack propagation and partially closed cracks were also studied using Calsyf. In the case of cracks subjected to traction–compression stresses that produce the partial closure of the crack, the open part can be obtained by equating the SIF to zero on the limit line where the crack closes.[10,15,16]

As an illustration of the accuracy of the method, two examples are given: an irregular crack in an infinite volume under uniform stress, named 'Guitel', and a surface

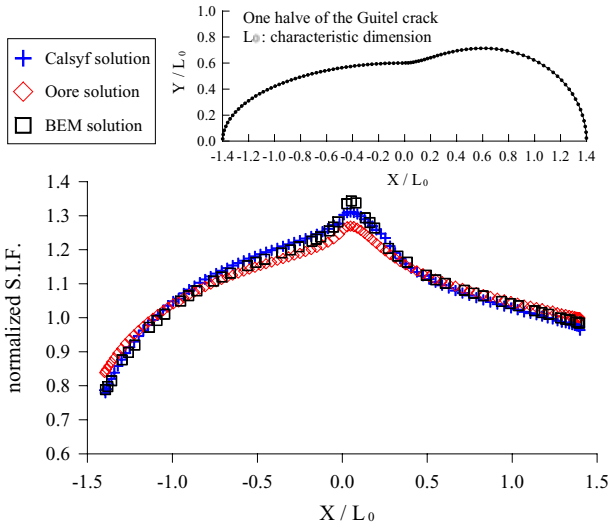

Fig. 7 Half of the 'Guitel' geometry and the normalized SIF at the crack front.

crack with semielliptical geometry under linear tension in a finite width plate. Figure 7 shows half of the Guitel geometry and the normalized SIF (see Eq. (4)) in the crack front, compared with results obtained by the boundary element method (BEM). A semielliptical crack of length a perpendicular to the free surface of a plate of thickness t under linear stress is shown in Fig. 8a (note the points of interest A and C), and Fig. 8b shows the normalized SIF at points A and C of semiellipses with different crack lengths, compared with the results of Newman–Raju,[13,14] Shiratori,[17] Glinka[18] and Isida.[19] The maximum relative error for the first case was near 2%, and the mean relative error of all the reported crack lengths, when comparing Calsyf and Newman–Raju results, was 0.23% for point A and 0.06% for point C in the second case.

$$K^N = K/\sigma\sqrt{\pi a}. \tag{4}$$

In the equation, σ is a characteristic stress and a is a characteristic crack dimension.

MODELS FOR CRACK GROWTH

The experimental evidence indicates that the propagation mechanism of the remaining crack is mechanical fatigue, characterized by a typical fracture surface with beach marks at the macroscopic level (see Figs 2 & 3), and striations at the microscopic level (see Fig. 4). Initiation took place by intergranular cracking from an original cast defect (see Fig. 3) up to the surface of the central hole in the upper part of the crosshead. This intergranular cracking was favoured by large inclusion defects at dendrite and grain boundaries (see Fig. 5).

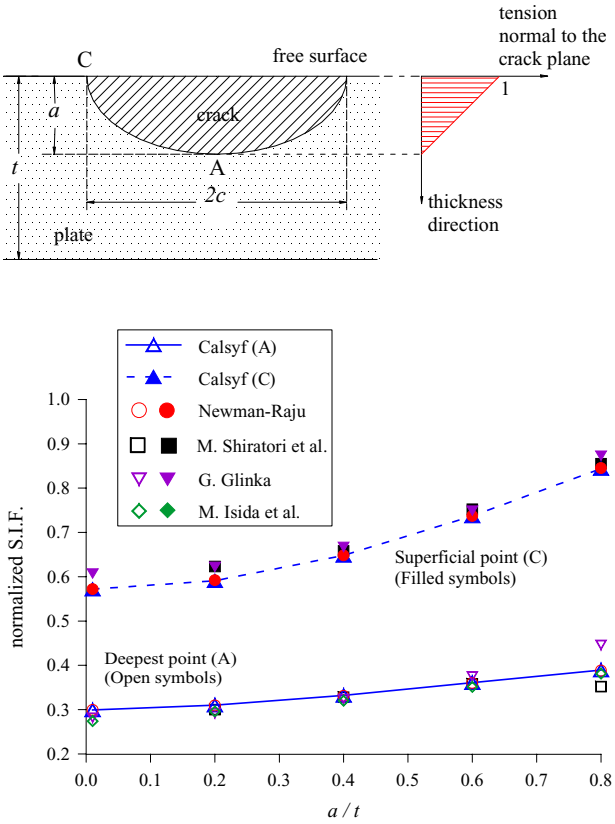

Fig. 8 (a) Semielliptical crack normal to the free surface of a plate under linear stress. (b) Normalized SIF at points A and C of semiellipses for different crack lengths.

The initial material defect is about 5 mm wide by 10 mm high (at the normal crosshead position) located about 4 mm from the OD of the centre hole and very close to the surface. Including the area with intergranular propagation, the entire initial defect is a roughly quarter elliptical corner crack, about 9 × 12 mm, breaking the surface of the central hole. Finite element calculations were carried out in order to determine if the actual operating conditions could justify the initiation of a fatigue crack from a pre-existing casting defect close to the central hole. The main parameters that were investigated are:

- When, why and how a true crack developed from the cast defect?
- For how long the remaining crack was propagating by fatigue from that original crack up to its final size?
- How the presence of this crack influenced the initiation and propagation of the main crack at the pinholes?

The approaches for the models are as follows. The assessment of the forces applied to the crosshead pin, considering pressure and dynamic loads, are shown in

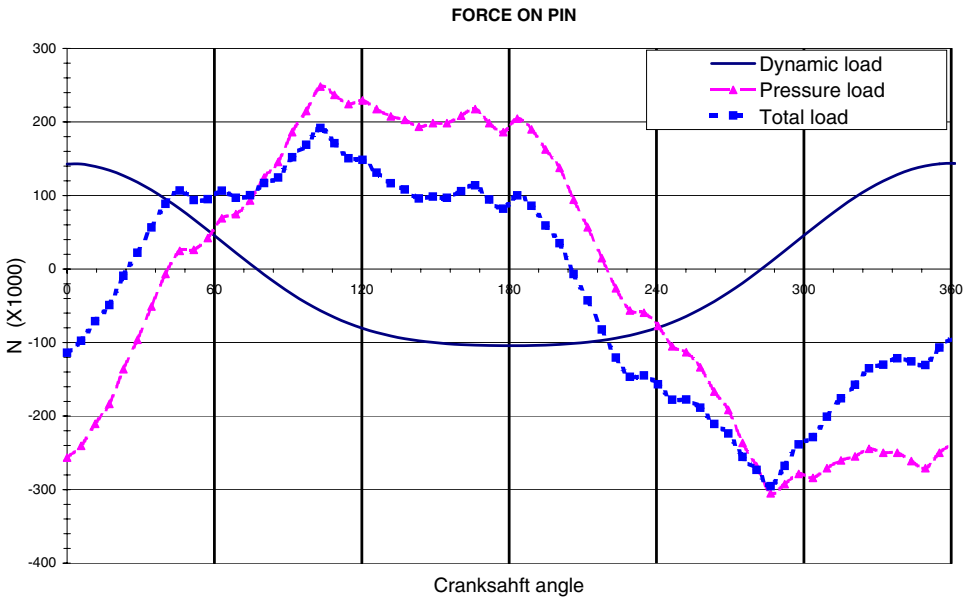

Fig. 9 Assessment of pressure and dynamic forces applied to the crosshead pin.

Fig. 9 as a function of crankshaft angle. The state of stresses and deformations in the crosshead were modelled for various conditions:

- Hydraulic preloads at each bolt in the rod clamping system between lower and upper limits according to DIN standard. Nominal hydraulic pressures in preloading assembly unit give load values between these two extreme cases.
- Nominal (45 mm) and actual (41 mm) crosshead thickness in the region of remaining crack.

The FEM distribution of maximum stresses in the vertical direction of the crosshead for both traction and compression piston cycles, is shown in Fig. 10a and b. The distribution of cyclic stresses normal to the remaining crack in the crosshead top is shown in Fig. 11. Only one half of the piston is analyzedanalysed, due to the symmetry of the problem and dimensions are given in millimetres and stresses in MPa. Conclusions drawn from these models are:

- Maximum tensile stresses in the hole area are around 240 MPa, but stresses drop drastically with distance from hole surface.
- Maximum cyclic stresses in the hole area are around 127 MPa.

Therefore, the stress state at the most severely stressed point on the hole surface is (176 ± 64) MPa. The maximum cyclic stresses in the hole area are $\Delta\sigma = 127$ MPa. As usual, propagation time can be estimated by using the cyclic stress intensity factor ΔK, applying the Paris equation for fatigue propagation and integrating from initial to final crack sizes.

The remaining crack is in a partially compressive stress field, which shows steep gradients in both directions in the crack plane. This geometry and load condition cannot be approximated using standard fracture mechanics formulas or tables, so it was modelled using a weight function based on integration of the Paris fatigue equation. This model allows the crack to partially close during certain parts of the fatigue cycle. The geometrical model, including the stress field from FEM, initial and final crack shapes, dimensions and normal-to-crack-plane stress distribution are indicated in Fig. 11.

The problem was modelled considering a coordinate system (s, u) as indicated in Fig. 11. The curved coordinate s is defined as the distance from the plane of symmetry along the circular inner surface of the piston; u is the distance in the radial direction, parallel to the z-axis. Stress amplitudes were obtained from the finite element results for the extreme nominal no-crack stresses applied normal to the cracked zone.

The geometry of the initial and final crack configurations together with the traction in the direction normal to the crack plane can be seen in Fig. 11. The area under analysis is restricted to the crack growth zone. The first two crack geometries studied were trapezoids, simulating an initial pre-existing defect. This is modelled by a 4 mm by 10 mm crack, 3 mm away from the hole surface, see Fig. 12. In a sensitivity analysis, the second trapezoid was reduced by half, leaving a 2 mm by 5 mm crack, also 3 mm away from the hole surface. The cyclic stress intensity factor range ΔK_I corresponding to the nominal operating range was

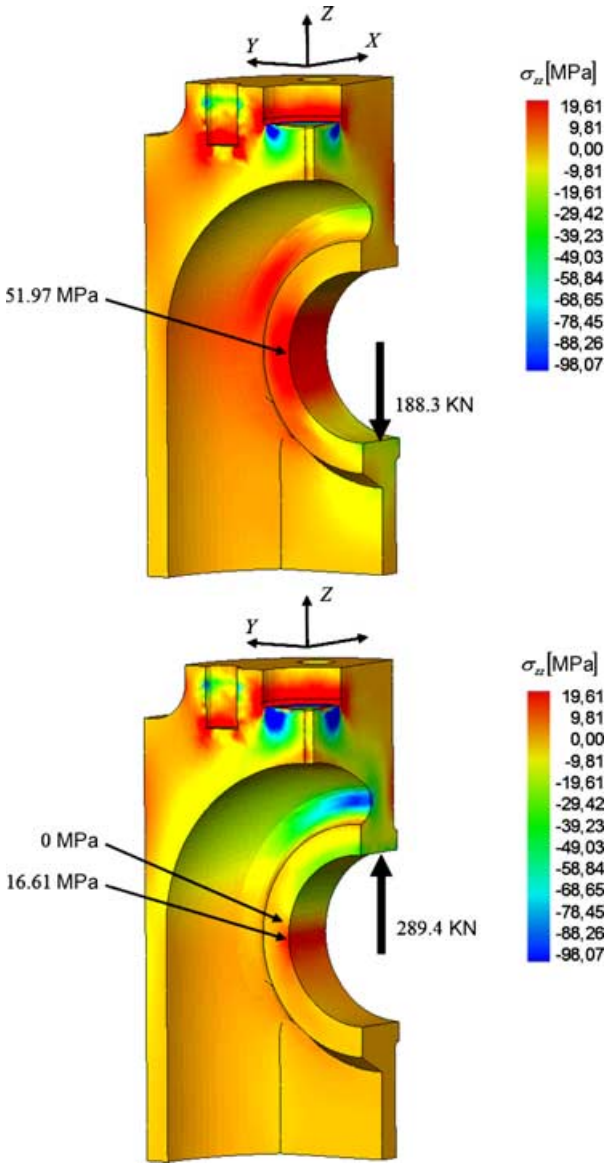

Fig. 10 Distribution of maximum vertical stresses in crosshead during traction (upper) and compression (lower) cycles.

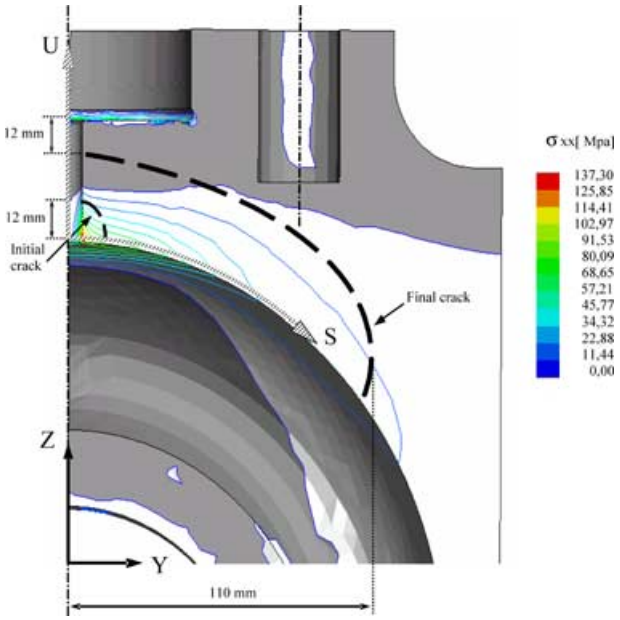

Fig. 11 Cyclic stresses, original and final shapes, and coordinate system for the remaining crack. Coordinate (x) is normal to the plane of the figure.

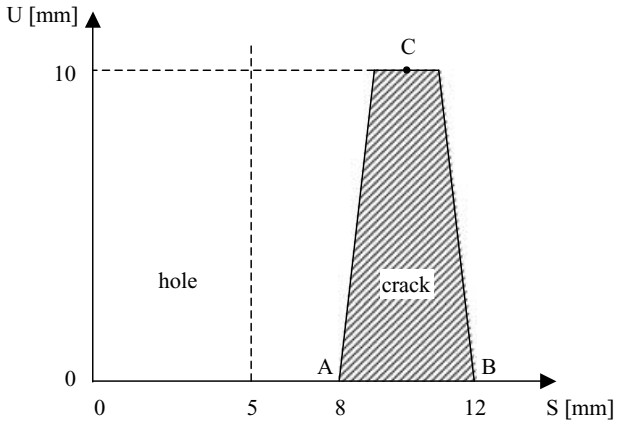

Fig. 12 Initial crack at top of crosshead modelled as a trapezoid.

studied for points on the surface and bottom of these initial cracks. Results are reported in Table 1, in MPa $\sqrt{m}$. Point A exhibits in both cases the maximum applied K_I values, which are well below the material fracture toughness. ΔK values for points A and B in both crack geometries are larger than the experimental fatigue threshold value.

Fatigue propagation of an initial semicircular crack of radius $r = 12$ mm was modelled using the Calsyf program. The semicircular crack models both sides of the crack, the 10-mm bore was modelled by considering zero stresses in a 10-mm strip of material. This leaves two symmetric quarter elliptical cracks, 7 mm by 9 mm, separated by the hole.

Experimental values for Paris constants and fatigue threshold were used. A preliminary study using the Calsyf program determined that the crack did not experience closure during its propagation. The evolution of the crack shape using Paris' law experimental parameters $C = 2.257 \times 10^{-8}$ mm/cycle, $m = 3.287$ and $\Delta K_{th} = 4.3$ MPa $\sqrt{m}$ is shown in Fig. 13. As can be seen in the figure, the aspect ratio of the crack decreases during its propagation, as well as the propagation rate. This is because the crack front evolves to regions of reduced nominal stresses. The relatively low value of ΔK_{th} experimentally found could be related to low roughness induced crack closure at low ΔK amplitudes, probably due to the small grain size of

Table 1 Stress Intensity Factors (MPa $m^{1/2}$) for cracks at a central hole, for cyclic and the maximum load at crosshead

Point in crack front	4 mm × 10 mm trapezoidal crack		2 mm × 5 mm trapezoidal crack	
	K_I for max. load MPa $\sqrt{m}$	ΔK_I for cyclic load MPa $\sqrt{m}$	K_I for max. load MPa $\sqrt{m}$	ΔK_I for cyclic load MPa $\sqrt{m}$
A	12.35	6.46	9.91	5.22
B	11.47	6.00	8.69	4.55
C	2.20	1.2	5.31	2.82

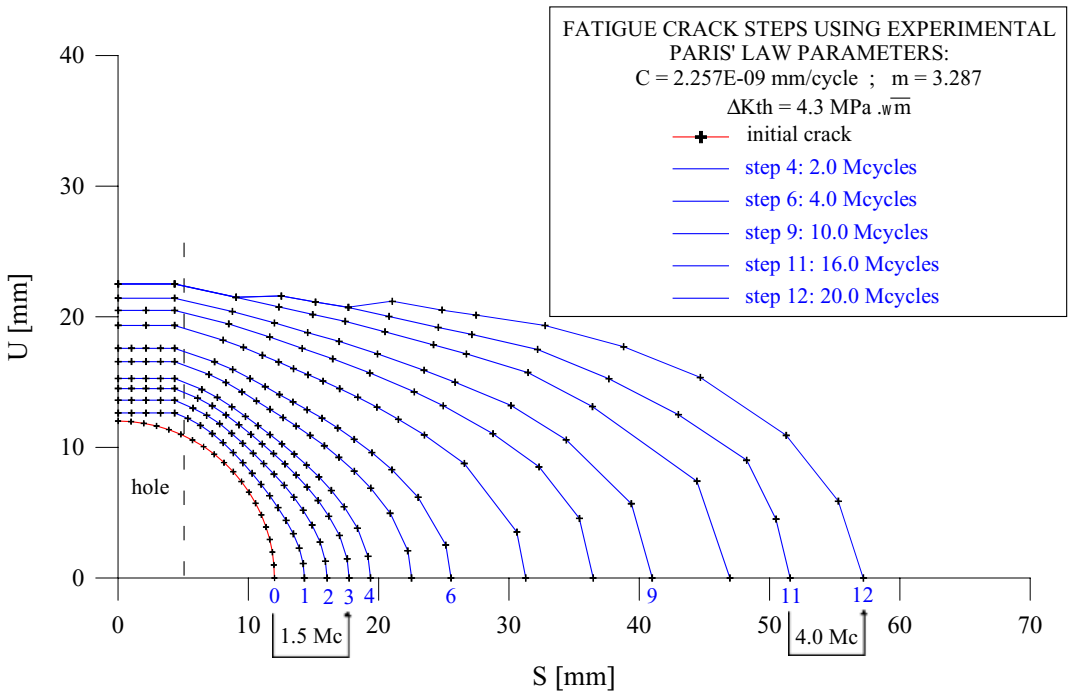

Fig. 13 Numerical prediction for fatigue growth of remaining crack.

the microstructure. The accuracy of C, m and ΔK_{th} is critical for the life estimates. The crack evolution considering ΔK_{th} causes the crack to not propagate near the hole when $u > 22$ mm, and therefore the crack depth remains almost constant (vertical direction in Fig. 13). Therefore, the value of ΔK_{th} affects the predicted evolution of crack shape. Although most crack growth occurs in the surface direction (horizontal in Fig. 13), values of ΔK for points in the crack front near the surface are very sensitive to crack depth.

It is easy to see that the crack propagation rate decreases in a monotonic fashion. For example, note from Fig. 13 that a crack extension of 5.7 mm was achieved in 1.5 million cycles in the first steps, meanwhile around 4 million cycles are necessary to propagate the same distance in steps 11–12. Using this data it is possible to extrapolate the total number of cycles to failure (given by the final crack shape shown in Fig. 11) to approximately 82.5 million cycles (see Fig. 14).

Note that the reduction of stresses in the crack front as the crack propagates is larger in the model than would be expected in reality. This is because the model does not take into account the reduction in the load bearing section as the crack propagates. This difference is small in normal cases because most of the fatigue life is spent when the crack is small. Our case is special because most of the fatigue life is spent by the growth of the crack when it is larger. This is because the applied stresses steeply decrease far from the initiation sites.

Striations and beach marks in some undamaged parts of the main crack between the pinholes indicate that this crack propagated by fatigue as a through-the-thickness crack. The fatigue crack propagated over the entire ligament from one pinhole to the other, that is, completed one half of the net section of the crosshead. The crack in the other half shows signs of fast fracture in most or all of its length. The simplest model used to evaluate if the normal operating loads were enough to produce this fast

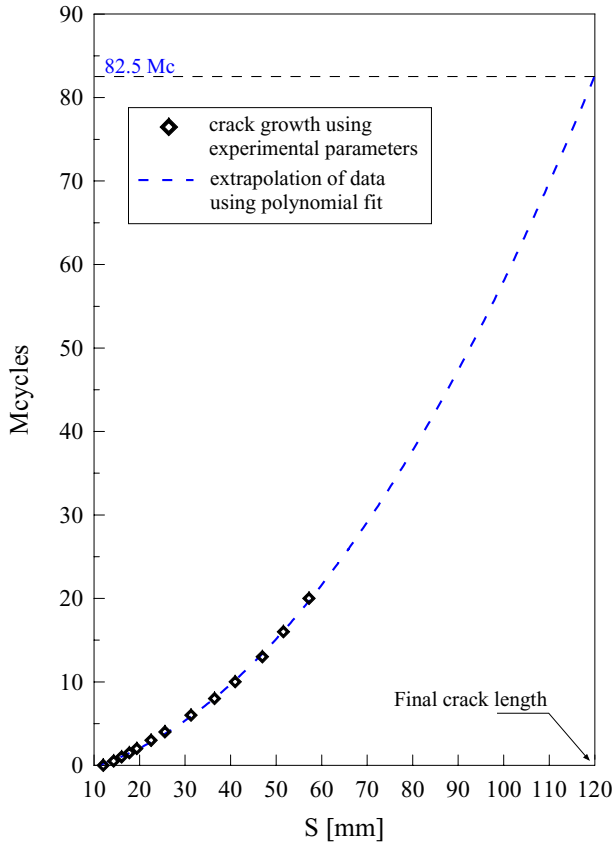

Fig. 14 Estimation of total number of fatigue cycles for final crack shape.

fracture includes a total downwards traction load applied to the pin of 250 kN. Maximum Von Mises equivalent stress at the pinhole surface is 350 MPa.

This is to say that as soon as the main crack, initiated at one pinhole, reached the surface of the other pinhole, the stresses at the uncracked surfaces of the pinholes were 10% larger than the yield strength of the material. This justifies initiation of plastic collapse of the remaining section. Therefore, it is concluded that the normal operating loads were sufficient to provoke the final failure of the crosshead. The maximum vertical opening of the full length fatigue crack prior to plastic collapse is 1.1 mm. Radial displacements of the cracked crosshead were also small enough to be accommodated within the gap between crosshead and liner.

DISCUSION OF RESULTS

The previous studies show that the failure of this large ethylene-reciprocating compressor was due to a perimetral crack developed between the pinholes in the crosshead of one of the cylinders. This crosshead and related parts were subjected to analysis, and several defects and abnormalities were identified. A subsurface cast void defect close to the central hole at the top of the crosshead propagated to initially form a 9 mm by 12 mm intergranular corner crack at the hole surface. This crack in turn propagated by fatigue, on both sides of the hole, creating what is called in this report, the remaining crack.

The lowest possible working temperature of the crosshead is room temperature, and occurs when it is first put into operation. In these conditions, the material is well within the ductile to brittle transition temperature range. Maximum applied stress at the initiation site has been estimated in 250 MPa, but drops drastically with distance from hole surface. Note that the yield strength is 320 MPa, is not that much higher.

Having severe segregation defects at the initiation site, it is conceivable that during this first cycle the maximum applied stresses could have propagated the initial 9 mm by 12 mm intergranular corner crack. It is difficult to provide more detail with respect to the exact early cracking mechanism. It is known that thin sulphide layers within the metal matrix have roughly the same yield strength of the metal matrix, but collapse as soon as the matrix is subject to minimal plastic deformation. This is because the thin layer is surrounded by stiffer material, creating a triaxial tensile stress state that delays the onset of plasticity (the same way the layer of solder behaves in a soldered joint). Phosphorus and sulphur levels in the crosshead material are around 150 ppm. Although not particularly high, these levels of impurities can justify the observed segregation of non-metallic impurities in grain boundaries during the solidification of the steel.

It is worth noting that the remaining crack is quite symmetric with respect to the central hole, although it was formed by the propagation of two cracks, one from each side of the hole (sites 1 and 2). Once the crack started in site 1, there was a progressive reduction of stiffness on that side of the hole. In a displacement-controlled situation, this leads to an increase of stress on the other side. When the crack had grown to a certain size, the stresses on the other side had increased to a level sufficient to initiate a second fatigue crack at a smaller defect, this is initiation site 2. When these two cracks continued to grow, the last to form was smaller but was being subjected to larger stresses, which lead to faster growth. In the end, both crack fronts levelled out.

Another interesting aspect when comparing actual pictures of the crack surfaces with the numerical results, is to see that the model was able to predict exactly the shape of the crack front during propagation.

FEM and fracture mechanics results give a cyclic stress intensity factor above the threshold level for fatigue crack growth. Integrating Paris equation for fatigue propagation from initial to final crack sizes, gives an estimated fatigue life of 80 million cycles. Therefore, this fatigue

crack should have initiated at least six months before the final failure took place.

The main fracture of the crosshead, the one that led to the final failure, occurred in a plane between the pinholes. Before fast fracture took place, this main crack propagated by fatigue over half the perimeter. The initiation site was lost due to plastic deformations after the main fracture occurred. The crack became unstable when it completed the ligament between the holes, at that moment the remaining ligament worked in bending, increasing the maximum tensile stress at the hole surface. As explained in the previous section, under normal operating loads this stress is larger than the material yield strength, which justifies the final fast propagation of the main crack.

An initial material defect, about 8 mm deep, was enough to initiate the fatigue growth of this main crack. The fatigue propagation time was around 50 million cycles. The remaining fatigue crack at the top, initiated at a material defect and was the first abnormality to propagate into the crosshead. There is, not necessarily, a cause and effect relationship between the remaining crack at the top and the main crack between the pinholes, both cracks could have been propagating simultaneously for some time during the service life of the compressor.

CONCLUSIONS

The main cause of the failure of a large rotating industrial component was identified as mechanical fatigue from manufacturing defects. This paper illustrates how a careful estimation of fatigue life for a crack of complex geometry, subjected to a complex stress field, allowed an understanding of the reasons for such an expensive failure. This estimate was carried out using a fast, versatile and reliable weight function-based numerical technique.

Acknowledgements

This research work was funded by the following Argentine Institutions: Agencia de Promoción Científica (PICT 12-04586), CONICET (Consejo Nacional de Investigaciones Científicas y Técnicas) and University of Mar del Plata (grant 15/G0379). The authors also wish to thank C. Hebert, A. Cisilino and P Barcia for their valuable contributions to this work.

REFERENCES

1 Failure analysis of compressor C111. Report GIE 2603-01/03, GIE S.A., Mar del Plata, Argentina, 2003.
2 Anderson, T. L. (1995) *Fracture Mechanics, Fundamentals and Applications*, 2nd edn. CRC Press, Boca Raton, FL.
3 "Standard Test Method for Measurement of Fatigue Crack Growth Rates," ASTM Designation E647-88. Vol. 03.01, 1988. ASTM Annual Standards, American Society for Testing and Materials. pp. 636–654.
4 Oore, M. and Burns, D. J. (1980) Estimation of stress intensity factors for embedded irregular cracks subjected to arbitrary normal stress fields. *Trans. ASME* **102**, 202–211.
5 Bueckner, H. F. (1970) A novel principle for the computation of stress intensity factors. *Z. Angew. Math. Mech.* **50**, 529.
6 Wu, Xue-Ren and Carlsson, A. J. (1991) *Weight Functions and Stress Intensity Factor Solutions*, 1st edn. Pergamon Press, Oxford, UK.
7 Khattab, M. A. A., Burns, D. J., Pick, R. J. and Thompson, J. C. (1986) Opening mode stress intensity factors for embedded rectangular and irregular planar defects. *J. Press. Vessel Techol.* **108**, 41–49.
8 Khattab, M. A. A., Burns, D. J., Pick, R. J. and Thompson, J. C. (1985) An integral technique to evaluate opening mode stress intensity factors for embedded planar cracks of arbitrary shape. *Trans. CSME* **9**, 1–10.
9 Desjardins, J. L., Burns, D. J. and Thompson, J. C. (1991) A weight function technique for estimating stress intensity factors for cracks in high pressure vessels. *J. Press. Vessel Technol.* **113**, 55–64.
10 Lopez Montenegro, H. (2002) Modelado por funciones de peso del comportamiento de fisuras bajo estados complejos de carga. Ph.D thesis, University of Mar del Plata.
11 Irwin, G. R. (1962) The crack extension force for a part-through crack in a plate. *ASME J. Appl. Mech.* **29**, 651–654.
12 Isida, M., Yoshida, T. and Noguchi, H. (1982) Preliminary Proceedings of the Japanese Society of Mechanical Engineers and Japan Society of Precision Engineering. Mie District, No. 823-3, pp. 15–17.
13 Newman, J. C. and Raju, I. S. (1981) An empirical stress intensity factor equation for the surface crack. *Eng. Fract. Mech.* **15**, 185–192.
14 Newman, J. C. and Raju, I. S., (1983) Stress intensity factor equations for cracks in three-dimensional finite bodies. Fracture Mechanics: Fourteenth Symposium – Vol. I: Theory and Analysis. In: ASTM STP 791 (Edited by J. C. Lewis and G. Sines). American Society for Testing and Materials, pp. I-238–I-265.
15 Woo, C .W., Cheung, Y. K., Chen, Y. Z. and Wang, Y. H. (1988) A simple model for the contact problem of a finite cracked plate in bending. *Eng. Fract. Mech.* **29**, 227–231.
16 Doblare, M., Espiga, F., Gracia, L. and Alcantud, M. (1990) Factores de intensidad de tensiones en problemas de cierre de grieta. *Revista Internacional de Metodos Mumericos para Cálculo y Diseño en Ingeniería* **6**, 261–284.
17 Shiratori, M., Miyoshi, T. and Tanikawa, K. (1986) Analysis of stress intensity factors for surface crack subjected to arbitrarily distributed surface stresses (2nd report, Analysis and application of influence coefficients for flat plates with a semielliptical surface crack), Trans. *Japan Soc. Mech. Eng.* **52**, 390–398.
18 Glinka, G. AFGROW program, version 4.0004.12.10. AFGROW web site, public service by the Analytical Structural Mechanics Brand, Air Vehicles Directorate, U.S. Air Force Research Laboratory.
19 Isida, M., Noguchi, H. and Yoshida, Y. (1984) Tension and bending of finite thickness plates with a semi-elliptical surface crack. *Int. J. Fract.* **26**, 157–188.